Noncontact Dipole Effects on Channel Permeation. II. Trp Conformations and Dipole Potentials in Gramicidin A

Andrea E. Dorigo,* Dean G. Anderson,# and David D. Busath#
*Department of Chemistry, Colby College, Waterville, Maine 04901, and #Zoology Department, Brigham Young University, Provo, Utah 84062 USA

ABSTRACT The four Trp dipoles in the gramicidin A (gA) channel modulate channel conductance, and their side chain conformations should therefore be important, but the energies of different conformations are unknown. A conformational search for the right-handed helix based on molecular mechanics in vacuo yielded 46 conformations within 20 kcal/mol of the lowest energy conformation. The two lowest energy conformations correspond to the solid-state and solution-state NMR conformations, suggesting that interactions within the peptide determine the conformation. For representative conformations, the electrostatic potential of the Trp side chains on the channel axis was computed. A novel application of the image-series method of Neumcke and Läuger (1969. *Biophys. J*. 9:1160–1170) was introduced to simulate the polarization of bulk water by the Trp side chains. For the experimentally observed structures, the CHARm toph19 potential energy (PE) of a cation in the channel center is −1.65 kcal/mol without images. With images, the PE is −1.9 kcal/mol, demonstrating that the images further enhance the direct dipole effect. Nonstandard conformations yielded less favorable PEs by 0.4–1.1 kcal/mol.

INTRODUCTION

Tryptophans are often located at the lipid-water interface in membrane proteins, where they are thought to orient the proteins in the lipid bilayer (Andersen et al., 1998). The Trp indole side chain has both polar and hydrophobic characteristics, the indole N-H bond in conjunction with a pair of conjugated rings providing a substantial dipole moment (2.1 Debyes), and the benzene ring being hydrophobic. This paper is the second in a series that focuses on the modulation of gramicidin channel current by interfacial dipoles, such as those produced by Trp and fluorinated Trp (Busath et al., 1998) side chains. Gramicidin A (gA) is a 15-amino acid polypeptide with the sequence formyl-V-G-A-D·L-A-D·V-V-D·V-W-D·L-W-D·L-W-D·L-W-ethanolamine, which dimerizes head to head to form channels in lipid bilayers. The eight Trps (residues 9, 11, 13, and 15 on each of two monomers) are located near the entry and exit of the twofold symmetrical channel (for reviews see Busath, 1993; Andersen and Koeppe, 1992; Woolley and Wallace, 1992; Killian, 1992). Because of the Trp dipole moments and positions, they modulate the flow of ions through the channel in lipid bilayers (Hu and Cross, 1995).

In general, six canonical Trp side-chain conformations are commonly observed in proteins, which include the two conformations seen with NMR in gramicidin, having $\chi^1 = 60°$ (G), $-60°$ (G′), or 180° (T) (the last two being equally common), and $\chi^{2,1} = +90°$ (+) or $-90°$ (−) (Richardson and Richardson, 1989). Depending on the backbone structure and adjacent side chains, many of the six canonical conformations may be inaccessible. For instance, in α-helices, the G′ and T conformations for χ^1 are equally populated by Trp, but G is rarely found, because the ring would intersect the helix, although on the inside surface of antiparallel β-sheets or either side of parallel β-sheets the G conformation is preferred for side-chain packing reasons (Richardson and Richardson, 1989).

The Trp indoles in gramicidin A have been found, using solution- and solid-state NMR, to be oriented with the N-H bonds facing the bulk water and their dipoles nearly aligned with the channel axis, and the positive end pointing toward bulk water in sodium dodecyl sulfate (SDS) micelles (Arseniev et al., 1986a) and dimyristoylphosphatidylcholine (DMPC) multilayers (Hu et al., 1993, 1995; Koeppe et al., 1994; Hu and Cross, 1995; Ketchem et al., 1996, 1997). For the right-handed $\beta^{6.5}$-helix gramicidin channel, two of the six canonical aromatic side-chain conformations (χ^1, $\chi^{2,1}$) have this property, namely (−60, −90°) and (180, 90°). In gramicidin channels, these two conformations have nearly identical orientations of the indole dipole and nuclear spin interaction tensors (the solid-state NMR observables) with respect to the plane of the bilayer.

Using solid-state NMR, the refined time-averaged χ^1 angles for Trp^9, Trp^{11}, Trp^{13}, and Trp^{15} were reported to be −74°, −71°, −64°, and −61°, respectively, and the $\chi^{2,1}$ angles were −82°, −91°, −85°, and −90°, respectively, with error bars of ±5° (Ketchem et al., 1997), all near a canonical −60°, −90° conformation. They fluctuated thermally with an rms amplitude between ±13° (Trp^{15}) and ±29° (Trp^{11}), primarily rotating about the $\chi^{2,1}$ axis (Hu et al., 1995). However, the solid-state data do not rule out a χ^1, $\chi^{2,1}$ conformation near a 180°, 90° canonical conformation. Vicinal H-Cα-Cβ-H coupling constants in the solution NMR results with gramicidin embedded in SDS micelles indicate that Trp^{11}, Trp^{13}, and Trp^{15} are near the −60°, −90° conformation, but that Trp^9 is 180°, 90° (Arseniev et al., 1985). Solution- and solid-state NMR studies with acy-

Received for publication 25 August 1998 and in final form 5 January 1999.
Address reprint requests to Dr. David Busath, Zoology Department, Brigham Young University, Provo, UT 84602. Tel.: 801-378-8753; Fax: 801-378-7423; E-mail: david_busath@byu.edu.
© 1999 by the Biophysical Society
0006-3495/99/04/1897/12 $2.00

lated gA suggest that Trp^9 is normally in the 180°, 90° conformation (Koeppe et al., 1995, 1996). However, Hu and Cross (1995) argued that Trp^9 is stacked in the −60°, 90° conformation with the indole plane parallel to that of Trp^{15} because both side chains have lower freedom than Trp^{11} and Trp^{13} (Hu et al., 1995) and because Trp fluorescence intensity is reduced in the channel conformation compared to that in the random coil conformation (Jones et al., 1986; Scarlata, 1988).

In Trp side-chain conformations in which the indole N-H projects toward the aqueous boundary, the axial indole dipole moment is expected on the basis of theoretical computations to enhance gramicidin channel conductance (Etchebest and Pullman, 1985; Sancho and Martínez, 1991; Hu and Cross, 1995; Woolf and Roux, 1997). Indeed, when the four Trps are replaced by phenylalanine, conductance of the analog channels is measurably diminished in diphytanoylphosphatidylcholine (DPhPC)/decane bilayers (Becker et al., 1991) as well as in monoolein (GMO)/hexadecane bilayers (Bamberg et al., 1976; Heitz et al., 1982, 1986, 1988). In addition, enhancement of the Trp dipole by fluorination at indole carbon-5 increases channel conductance to Na^+ and K^+ (Andersen et al., 1998; Busath et al., 1998), but only under conditions in which translocation through the channel is the process that limits the rate of current flow (Busath et al., 1998).

The main factors expected to affect Trp conformation include at least four types of interactions: with backbone and adjacent side chains (including other Trp dipoles), which we will refer to as conformational energy; hydrophobic forces on the indole aromatic rings; interactions such as hydrogen bonds between the polar indole N-H and lipid headgroups or water; and the electrostatic interaction between the indole dipole of 2.1 D (Weiler-Feilschenfeld et al., 1970) and the interfacial dipole potential of 274–390 mV (Pickar and Benz, 1978) spread over a headgroup layer thickness of >6 Å (Dilger, 1981).

Before measurement of the side-chain conformations in gramicidin, a conformational search based on a proprietary force field was reported (Venkatachalam and Urry, 1983). Side-chain dihedrals were spaced at 30° intervals, and energies of interaction with backbone and other side chains for viable Trp conformation sets were reported. Using a left-handed helix, four independent conformations for Trp^{11}, three for Trp^{13}, and four interdependent sets of Trp^9/Trp^{15} conformations with interaction energies within 5 kcal/mol per residue were identified. The optimal conformation for the left-handed helix was used for subsequent computations (Roux and Karplus, 1988; Turano et al., 1992), and the entire set was used to analyze Raman spectroscopy results (Takeuchi et al., 1990), but unfortunately, the set did not include the solid- and solution-state NMR conformations discovered subsequently. Furthermore, NMR demonstrated (Arseniev et al., 1986a,b; Nicholson and Cross, 1989; Separovic et al., 1994) that the helix was right-handed rather than left-handed. In this backbone conformation the Trp side chains project more toward the aqueous bath because of the angle of the Cα-Cβ bond with the helix axis (Nicholson and Cross, 1989). Although Venkatachalam and Urry (1983) identify a minimum energy side-chain conformation for a right-handed helix, they give no details of a conformational search with the right-handed helix. Consequently, we decided to revisit the conformational search, using the right-handed helix and a standard force field.

Here we report the results of a conformational search study using the CHARMm force field. Like the Venkatachalam-Urry analysis, we explored a limited set of starting conformations, consisting in our case of just the canonical conformations; but we also minimized each starting configuration, producing a somewhat more robust search of conformational space. The lipids and waters in the environment, which are expected to affect the energetics of the Trp-side-chain orientations that differ with respect to the plane of the interface, were not included, to focus on the conformational requirements of the peptide. We show below that the solid-state and solution-state NMR structures are among the three lowest energy structures that emerged from the calculations.

Then, in conjunction with a larger project to analyze the effects of side-chain dipoles on ion transport in gramicidin, we compute the electrostatic potential of the indole dipole (direct component) and its associated bulk water reaction (indirect component) at the channel axis for different Trp conformations. The indirect component is based on the method of images (Weber, 1965; Neumcke and Läuger, 1969; Hao et al., 1997; Iverson et al., 1998). The electric field of an ion in a slab of low-dielectric medium (lipid) sandwiched between two high-dielectric semiinfinite slabs (water) is represented by the charge and its images in a uniform low-dielectric medium. Within the bilayer, the field of the image charges embedded in a uniform low-dielectric medium is equivalent to the field of the high-dielectric medium polarized by the charge in the bilayer. The interaction between the ion and the image charges was introduced to compute the self-energy (or image potential) barrier (Neumcke and Läuger, 1969) for the aqueous dielectric reaction to an ion passing through the membrane, which represents the majority of the saline reaction (Jordan et al., 1989). We apply the same method to represent the bulk water reaction to Trp side chains in the membrane and then calculate the interaction energy between an ion in the channel and the image charges to obtain the indirect component. A more elegant analytical method derived by Smythe (1967) was also implemented, but the image charge approach proved to be accurate and more efficient. Although an atomistic approach (i.e., using explicit dynamic solvent waters) might seem preferable, in practice the mesoscopic approach is necessary for this problem because of the low energies involved.

The electrostatic potential of the indoles contributes to the total electrochemical potential, which also includes interactions between the ion and all other components of the environment (aqueous bath solvent, channel waters, channel backbone and nonpolar side chains, and lipid molecules)

(Jordan, 1984), as well as energy effects of ion-induced changes in the average conformation of surrounding molecules. Ion permeation is an electrodiffusive process, approximately divisible into three main steps because of general features in the electrochemical potential profile: diffusion up to a binding site just inside the channel entrance, diffusion to the symmetrical site near the exit, and diffusion away from the channel. For permeant ion concentrations greater than ~200 mM and at membrane potentials less than ~200 mV, channel conductances are limited by the middle transport step, translocation through the channel, judging from the shapes of current voltage relationships (Hu and Cross, 1995; Busath et al., 1998). Although the Trp potential of mean force (PMF) affects other aspects of transport, especially ion binding, here we focus primarily on modulation of the translocation step that results from reduction of the barrier to translocation by the outward-pointing Trp dipoles.

Although it is straightforward to estimate the ion-dipole interaction energy from Coulomb's law, it is more difficult to accurately estimate the dielectric shielding produced by the nearby polar structures: lipid headgroups, peptide backbone, and pore waters. Proteins are often estimated to have an overall dielectric constant of ~25, but the hydrogen-bonded, hydrophobic interior of proteins is generally estimated to have a value near 4 (e.g., Simonson, 1998; Sham et al., 1998). We assume that the strongly hydrogen-bonded β-helix backbone presents a dielectric constant as low as 4, and possibly as low as the atomic polarizability limit of ~2. Likewise, pore waters have often been modeled as a high-dielectric medium with $\epsilon = 80$, like bulk water, but channel ions completely orient channel waters (Partenskii et al., 1991) so that the residual dielectric response probably corresponds to a dielectric constant of 2–4. The polar headgroups are thought to have properties intermediate between those of lipid tails ($\epsilon = 2$) and bulk water. For simplicity, we treat the polar headgroup region as indistinguishable from bulk water.

We find that the translocation barrier would be less reduced for the conformations in which one or more Trp side-chain N-H bonds project toward the center of the bilayer rather than toward the bulk water, so that these conformations should have reduced single-channel conductance compared to the two NMR-derived conformations, at least under conditions where the translocation barrier limits current flow in the channel.

METHODS

Parameters

The calculations in this paper were performed using CHARMm (Molecular Simulations, San Diego, CA) with the toph19 charges and param19 parameters (Brooks et al., 1983). In particular, the partial charges on the Trp side chain were C^{β} 0.00, $C^{\delta 1}$ 0.06, C^{γ} −0.03, $N^{\epsilon 1}$ −0.36, $H^{\epsilon 1}$ 0.30, $C^{\delta 2}$ 0.10, $C^{\epsilon 2}$ −0.04, $C^{\epsilon 3}$ −0.03, $C^{\zeta 2}$ 0.00, $C^{\zeta 3}$ 0.00, $C^{\eta 2}$ 0.00 (atom names according to IUPAC convention; IUPAC-IUB, 1970). This charge distribution corresponds to a dipole moment of 1.15 D at an angle of 43° to the inter-ring bond. The value of the dipole moment differs considerably from that measured in benzene, 2.1 D, and the angle differs somewhat from the reported value of 50° (Weiler-Feilschenfeld et al., 1970). Therefore, ion-dipole energies reported here should be scaled up by a factor of at least 1.8 to correct for the low dipole moment inherent in the toph19 fixed partial charge distribution. Some uncertainty is also to be expected based on a discrepancy of ~7° in the angle of the dipole relative to the indole position and neglect of the polarization of the Trp indole by the passing ion.

Gramicidin backbone structure

The structure for the gramicidin backbone and side chains was obtained from the proton-NMR-based dihedral angles and docking parameters for the peptide incorporated in dodecylsulfate micelles in the head-to-head single-helix channel conformation (Arseniev et al., 1986a). The dimer geometry was refined in a vacuum by means of energy minimization to an atomic RMS energy gradient less than 0.1 kcal/mol.

Side-chain conformational analysis

First an ensemble of the (6^4) possible combinations of six canonical rotameric orientations for the four Trp side chains was generated using CHARMm. The dihedral χ^1 was assigned values of 180, 60, or −60°; $\chi^{2,1}$ was assigned values of ±90°. Twofold symmetry was assumed, i.e., the starting rotamer conformation was the same for each monomer in the dimeric channel. The Trp side chains and backbone were fixed for 50 cycles of energy minimization to relax the non-Trp side chains. The resulting conformers with steric energies higher than 1000 kcal/mol were discarded. In the discarded conformations, which represented the vast majority, at least one Trp group overlapped another side chain or the backbone. This procedure had the effect of focusing only on the viable canonical Trp conformations at this stage of the search.

Optimization of the viable conformations was then carried out with all side chains free and backbones fixed until their energy gradient was lower than 0.1 kcal/mol. In this step, the optimal Trp dihedrals nearest the canonical conformations were obtained. Generally, the χ^1 dihedrals remained within ~15° and $\chi^{2,1}$ within ~40° of the starting conformation. The 46 conformers with the lowest energy were kept for analysis. One hundred additional cycles of optimization using the same constraints resulted in small energy changes, typically less than 2 kcal/mol, for each of the 46 conformers. The optimization criteria therefore appeared acceptable.

Classification of Trp conformations

In discussing the results of our calculations, we first regroup the Trp indole conformations according to whether the indole dipole points toward the bulk water (o), toward the center of the bilayer (i), or parallel to the plane of the bilayer (p). This classification emphasizes the expected effects on channel conductance and is illustrated in Fig. 1, which shows the six canonical Trp conformations for Trp^{13}, three in each of two channels for clarity, relative to the channel backbone, which is oriented normal to the lipid bilayer. For the case of the right-handed helix, G′− and T+ point out (o), G′+ and T− point in (i), and G+ and G− are parallel (p) to the bilayer plane. (The left-handed helix differs because the backbone is rotated ~180°.) The three classes, o, i, and p, are subdivided for the seven most energetically favorable structures in each group, based on whether $\chi^{2,1}$ is negative (1) or positive (2).

We further group the channel monomer conformations according to whether zero (group 0), one (group 1), or two (group 2) Trps are pointing in or are parallel. Although it is also possible that three or four could point in or parallel to the channel, no examples occurred in our search. This grouping again anticipates the effect on conductance, as the members of each channel monomer conformation group are expected to yield similar axial electrostatic potentials.

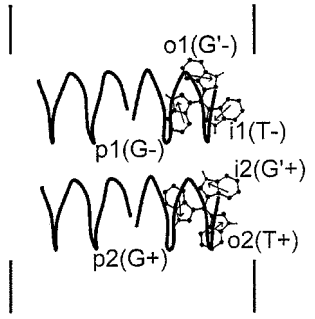

FIGURE 1 Six canonical Trp[13] side-chain configurations for gramicidin A dimer. The channel backbone is represented by a cartoon. The indole dipoles are shown in representative positions projecting either toward the aqueous solution (o1 and o2), toward the bilayer (i1 and i2), or parallel to the bilayer (p1 and p2).

Solvent reaction image charges

The axial electrostatic potential was calculated (see below) both in vacuo and with an additional solvent reaction field to simulate reaction of the bulk water to the Trp conformations. For the reaction field, an additional set of point charges, located outside the channel, is included in the calculations to represent the electrostatic effect of the Trp side chains mediated by the polarization of bulk water. The image charges, q and q', and their positions, x and x', were computed using the equations of Neumcke and Läuger (1969). For each Trp atomic partial charge, q_i, located in the membrane at position $0 < x_i < d$, where d is the membrane thickness, there are four series of image charges:

$$q_{-n} = \theta^{2n+1} q_i \text{ at } x_{-n} = -2dn - x_i \quad (n = 0, 1, 2, \ldots) \quad (1)$$

$$q_n = \theta^{2n-1} q_i \text{ at } x_n = 2dn - x_i \quad (n = 1, 2, 3, \ldots) \quad (2)$$

$$q'_{-n} = \theta^{2n} q_i \text{ at } x'_{-n} = -2dn + x_i \quad (n = 1, 2, 3, \ldots) \quad (3)$$

$$q'_n = \theta^{2n} q_i \text{ at } x'_n = 2dn + x_i \quad (n = 1, 2, 3, \ldots) \quad (4)$$

where the parameter $\theta = (\epsilon_1 - \epsilon_2)/(\epsilon_1 + \epsilon_2)$ is computed from the dielectric constants outside ($\epsilon_2 = 80$) and inside ($\epsilon_1 = 2$) of the bilayer. Note that the first pair of charges, q_{-n} and q_n, have signs opposite those of q_i and represent the primary images in the two solvent baths. The second pair, q'_{-n} and q'_n, are the opposite of the first pair and are second-order images, i.e., images of the first-order images in the solvent bath on the opposite side of the lipid bilayer. The equations describe an infinite series of image charges, but the axial electrostatic potential from the images beyond the fourth-order images was negligible, and the series was truncated at this level.

In Fig. 2 the dielectric regions used for the image charge calculations

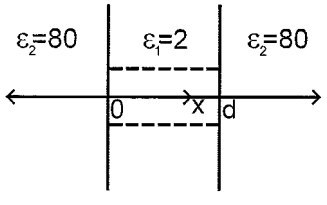

FIGURE 2 The dielectric regions used in the computation of the image charges. A bilayer of thickness d is assigned a dielectric constant of 2 throughout, including the channel region, which is shown by dashed lines. The aqueous solution on either side is assigned a dielectric constant of 80. The axial positions of charged indole atoms in the bilayer are denoted by x.

are defined as 80 in the aqueous solution and 2 in the bilayer, the channel walls, and the channel interior. In Fig. 3 the gramicidin channel is represented by a backbone cartoon with Trp side chains in the o1 positions, i.e., with indole N-H hydrogens projecting toward the aqueous bath. On the left and right are the images of the Trp side-chain atoms (as defined above), representing $n = 0$ and $n = 1$ in Eqs. 1 and 2, respectively. Because of sign reversal in the first order images, the image dipoles are opposite those of the real charges. Consequently, the closest and most significant image dipoles are parallel, rather than antiparallel, to the real charges and enhance the effect (agonistic or antagonistic) of the real charges. The positions of the image charges were dependent on the choice of the location of the interface, which was somewhat arbitrary. The channel itself is 25 Å long, but the low-dielectric region can be longer, because the lipid groups extend beyond the edge of the channel. For our calculations we arbitrarily assumed a hydrophobic thickness of $d = 31.0$ Å, similar to that measured using membrane capacitance for the GMO/hexadecane bilayer, 32.7 Å (Dilger, 1981) and ~33 Å (Waldbillig and Szabo, 1979).

PMF calculation

To compute the mean force potential exerted by the Trp side-chain atomic partial charges on a monovalent cation moving along the axis of each conformer, a Na^+ ion was located at each of 601 equally spaced positions along the channel axis between −15 and +15 Å. The Coulombic electrostatic energy between the ion and each Trp side chain was computed with CHARMm, using no nonbonded pair cutoffs and a dielectric constant of 2 representing the polarizability of the lipid, peptide, and channel water atoms in the vicinity of the Trp indoles (see Fig. 3). In this paper, we do not estimate changes in ion flux predicted by the computed PMFs, preferring to leave this until a more accurate PMF is obtained with better Trp charges and with inclusion of the interaction energy between ion-polarized channel waters and Trp side chains. Instead, the discussion focuses on a comparison with previous estimates of the Trp PMF on the channel axis, one based on experiment and three based on quite different theoretical approaches.

RESULTS

Table 1 lists the members of the three Trp conformational groups from the conformational search performed in vacuum, which have zero (group 0), one (group 1), or two (group 2) inward or parallel pointing side chains in each monomer, and their conformational potential energies. The side chains of corresponding residues from the two monomers, although minimized independently, generally had approximately the same final conformations. The energies consist of side-chain strain, side chain–side chain interac-

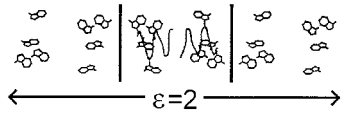

FIGURE 3 Charge images of the Trp side chains are shown to the left and right of a channel. Those on the left are reflections of the original side chains about the left lipid-water interface and are positioned and charged according to Eq. 1 at $n = 0$. Those on the right are reflections about the right lipid-water interface and are calculated according to Eq. 2 at $n = 1$. The image charge approach replaces the lipid-water boundaries with an infinite series of image charges and a dielectric constant of $\epsilon 2$ throughout. The images shown here represent the first two of 16 sets of images used in the calculations in this paper; the other 14 sets are located at progressively further distances from the original channel.

TABLE 1 Calculated conformation energies, by peptide conformation group, from modeling based on the SDS micelle right-handed helix backbone

Conformer	Energy (kcal/mol)	Trp residue orientation			
		9	11	13	15
Group 0					
1	−32.0	o1	o1	o1	o1
2	−31.1	o2	o1	o1	o1
3	−22.9	o1	o1	o1	o2
4	−21.8	o1	o1	o2	o1
5	−19.5	o2	o1	o2	o1
6	−14.3	o2	o1	o1	o2
7	−12.0	o1	o1	o2	o2
Group 1					
8	−30.7	i1	o1	o1	o1
9	−25.8	i2	o1	o1	o1
10	−23.6	o1	o1	i2	o1
11	−23.6	o1	p1	o1	o1
12	−22.7	o1	o1	o1	i2
13	−21.9	o1	i1	o1	o1
14	−21.7	o1	o1	i1	o1
15	−21.3	o	o	o	i
16	−20.6	o	p	o	o
17	−19.4	o	o	i	o
18	−19.4	o	o	i	o
19	−18.5	o	i	o	o
20	−17.8	i	o	o	o
21	−17.6	o	o	o	i
22	−17.4	i	o	o	o
23	−15.8	o	o	o	i
24	−15.7	o	p	o	o
25	−15.0	o	i	o	o
26	−14.6	o	o	i	o
27	−14.2	i	o	o	o
28	−13.4	o	i	o	o
29	−12.5	o	o	o	i
30	−12.0	o	o	i	o
Group 2					
31	−19.3	i1	p1	o1	o1
32	−19.2	i1	o1	o1	i2
33	−18.0	i2	o1	i2	o1
34	−17.8	i1	o1	i2	o1
35	−17.4	i2	p1	o1	o1
36	−17.3	i1	o1	i1	o1
37	−16.7	i1	p1	o1	o1
38	−15.5	i	o	o	i
39	−14.6	i	i	o	o
40	−14.4	o	i	o	i
41	−14.4	i	o	i	o
42	−14.3	o	o	i	i
43	−13.6	i	o	o	i
44	−13.4	o	i	i	o
45	−12.6	o	p	o	i
46	−12.3	o	o	i	i

tion, and side-chain backbone interaction energies but not backbone bond or nonbond energies.

Table 2 gives the mean and standard deviation of the dihedral angles for each o, i, and p subclass represented in the conformation set. The means are close to canonical conformation values, and the standard deviations are relatively small.

Channel monomer conformation 1 from Table 1 has o1 positions for all four Trps, which corresponds to one possible solid-state NMR structure. Conformation 2 has o2 at position 9 and o1 at the other three positions, corresponding to the solution NMR structure. Other structures have higher energies, indicating less favorable interactions between the side chain and the rest of the peptide. However, structure 8, with i1 at position 9, has essentially the same energy as structures 1 and 2 and would certainly be expected to occur in the bilayer environment unless hydrogen bonding, hydrophobic, or dipole-interfacial potential interactions destabilize it relative to the other two. The conformational energies suggest that many of the other conformations might also be observed occasionally if stabilized by the environment or high barriers to interconversion.

Fig. 4 *a–d* (*no symbols*) shows the ion-Trp interaction energy profiles for conformers 1, 8, 31, and 46 of Table 1. Conformers 1, 8, and 31 are the most stable conformations of their respective groups in Table 1. Conformer 46 (Trp^{9} and Trp^{11}, o1; Trp^{13}, i1; Trp^{15}, i2), though the least stable conformer in group 2, is shown because it illustrates a conformation opposite that of conformer 31 (Trp^{9}, i1; Trp^{11}, p1; Trp^{13} and Trp^{15}, o1). The conformations with more N-H groups pointing outward yield greater stabilization of the cation at the center of the channel. The cation is stabilized at the center by 1.8 kcal/mol when all four groups point outward (structure 1), but this stabilization energy drops to 1.4 kcal/mol when only three groups point outward (structure 8) and to 0.7 kcal/mol when only two groups point outward (structures 31 and 46). There is also some variation in the shape of the interaction energy profile, with an 0.6 kcal/mol central hill in the Trp PMF for structure 31, which is negligible in the other three cases.

The image PMF (Fig. 4, *a* and 4 *d*, *no symbols* versus *symbols*) either enhances or reduces the Trp stabilization energy, depending on the side-chain conformation. In Fig. 4 *a*, where all eight Trps are in the o1 conformation (which stabilizes the cation in the center of the channel, i.e., contributes an energy well to the total energy profile), the image PMF deepens the total PMF because charge reversal in the images results in parallel alignment with the real dipoles for the nearest image dipoles (Fig. 3). In Fig. 4 *d*, where two of the pairs of Trps (Trp^{13} and Trp^{15}) are in the i1 configuration which destabilizes the cation in the center of the channel, the image PMF further destabilizes the ion. In this case, the destabilizing images (13 and 15) are nearer the center of the channel than the stabilizing images (9 and 11), and their effect dominates. Interestingly, in this case, the destabilizing effect of the images is greater at the ends of the channel ($x = \pm 12.5$ Å) (which are near the main cation-binding sites, $x \approx \pm 10$ Å), than at the center ($x = 0$ Å), because of the proximity of the destabilizing image dipoles to the binding site.

Variations in profiles among o1 and o2 conformers are modest, as shown for group 0 (Fig. 5 *a*). In group 1 (Fig. 5 *b*), one pair of side chains is rotated to the i or p state for each structure, so the stabilizing energies at the center are

TABLE 2 Mean (± SD*) χ^1 and $\chi^{2,1}$ (in degrees) for Trp conformation types#

	Trp^9		Trp^{11}		Trp^{13}		Trp^{15}	
	χ^1	$\chi^{2,1}$	χ^1	$\chi^{2,1}$	χ^1	$\chi^{2,1}$	χ^1	$\chi^{2,1}$
o1 (G′−)§	−70.2 ± 1.7	−68.4 ± 7.1	−55.2 ± 2.1	−66.2 ± 2.2	−56.0 ± 0.8	−74.0 ± 2.1	−58.0 ± 2.3	−75.3 ± 4.7
o2 (T+)	−175.0 ± 3.0	80.7 ± 10.5	N.O.¶	N.O.	−164.1 ± 0.8	74.4 ± 1.3	−176.2 ± 3.8	86.5 ± 3.5
i1 (T−)	−178.3 ± 2.5	−88.1 ± 2.9	−171.1 ± 3.1	−130.3 ± 0.5	−175.9 ± 2.8	−125.9 ± 8.6	N.O.	N.O.
i2 (G′+)	−60.0 ± 1.4	93.2 ± 5.3	N.O.	N.O.	−58.0 ± 0.9	101.8 ± 2.6	−60.6 ± 2.6	102.2 ± 5.8
p1 (G−)	N.O.	N.O.	48.3 ± 1.0	−78.0 ± 2.1	N.O.	N.O.	N.O.	N.O.
p2 (G+)	N.O.	N.O.	N.O.	N.O.	N.O.	N.O.	N.O.	N.O.

*The standard deviation of the dihedral angles among all of the conformers listed in Table 1, with the canonical conformation specified in parentheses.
#The minimum energy values from both monomers for each of the 21 subclassified conformations listed in Table 1 are averaged.
§The starting conformations (before minimization) are the canonical conformations in parentheses labeled according to the scheme of Takeuchi et al. (1990).
¶N.O., Not observed.

1.2–1.4 kcal/mol compared to 1.7–1.9 kcal/mol in group 0. Inward or parallel configurations of one of the side-chain pairs are thus expected to result in a loss of ~0.3–0.7 kcal/mol of cation stabilization at the center of the channel, depending on which residue is rotated.

The contributions of the individual side-chain pairs are shown for some o, i, and p conformations for each of the four Trp pairs in Fig. 6. The depth of the stabilization well for the o1 conformer is similar for all four side-chain pairs in conformation 1, as shown by the curves without symbols in the four panels (~0.5 kcal/mol). However, the shape varies as expected with the axial position of the side chain, that is, Trp^9 (Fig. 6 *a*) contributes a narrow well with complete merger of the profiles from the two monomer contributions, whereas Trp^{15} (Fig. 6 *d*) contributes a broader well with incomplete merger. The o2 configuration (from conformation 2) yields a PMF comparable to the o1 conformation (Fig. 6 *a*, *triangles*).

If some Trp side chains were to assume an inward-pointing conformation, their electric fields would oppose those of the remaining outward pointing side chains, as shown in the curves with circles in Fig. 6. Fig. 6, *a* and *b*, contains the PMFs for Trp^9 in the i1 configuration and Trp^{11}

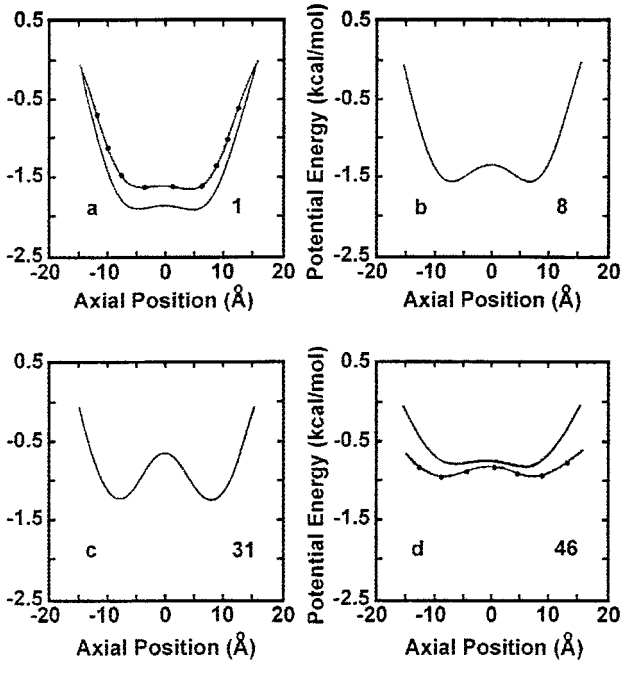

FIGURE 4 The PMF along the channel axis due to interactions between a cation and all eight Trps and their images are shown for four representative conformations obtained from the conformational search. (*a*) Conformation 1 (all Trps in the o1 position). (*b*) Conformation 8, in which the pair of Trp^9's is i1 and the other three pairs are o1. (*c*) Conformation 31, in which the pair of Trp^9's is i1, the pair of Trp^{11}'s is p1, and the other two pairs are o1. (*d*) Conformation 46, in which the pair of Trp^{13}'s is i1 and the pair of Trp^{15}'s is i2 with the other two pairs are o1. In *a* and *d*, the PMFs computed from the Trps alone without images are marked by symbols.

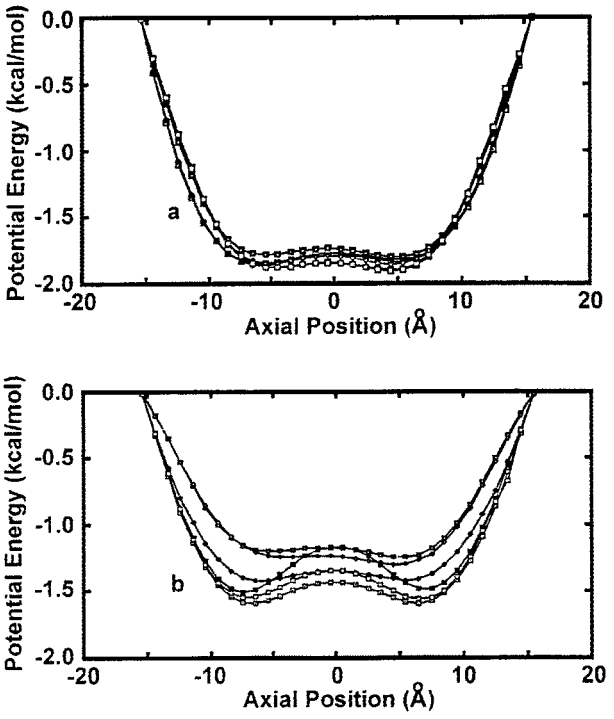

FIGURE 5 The PMF, image PMF included, for individual conformations. (*a*) All eight of the group 0 conformations from Table 1, in which all eight Trps are in the o (outward pointing) position. (*b*) Conformations 8–14 from group 1 in Table 1, in which one of the four Trp side chains on each monomer is in the i (inward pointing) or p (perpendicular to axis) position.

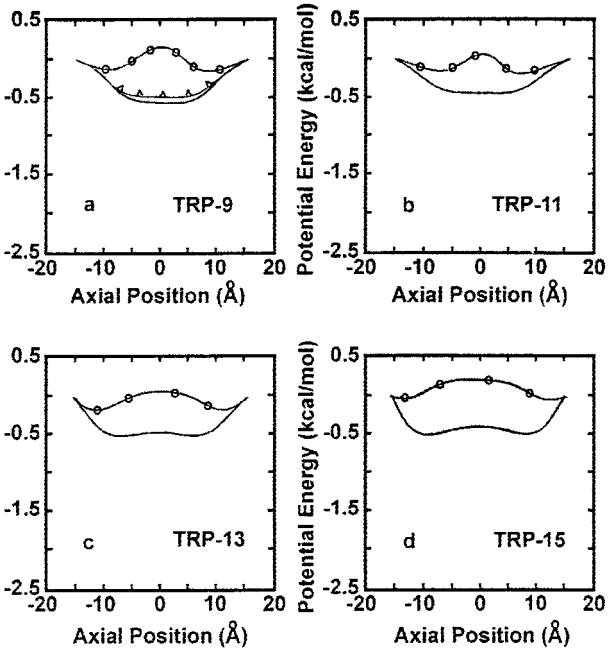

FIGURE 6 PMFs, image PMF included, of individual pairs of Trps are compared for o1 and alternative positions. (*a*) The Trp^9 PMF from conformation 1 (o1, *no symbols*) is compared to that of conformation 2 (o2, △) and to that of conformation 31 (i1, ○). (*b*) The Trp^{11} PMF from conformation 1 (o1, *no symbols*) is compared to that of conformation 31 (p1, ○). (*c*) The Trp^{13} PMF from conformation 1 (o1, *no symbols*) is compared to that of conformation 46 (i1, ○). (*d*) The Trp^{15} PMF from conformation 1 (o1, *no symbols*) is compared with that of conformation 46 (i2, ○).

in the p1 configuration, both from conformation 31. Fig. 6, *c* and *d*, contains the PMFs for Trp^{13} in the i1 configuration and Trp^{15} in the i2 configuration from conformation 46. The dipole potential is destabilizing at the center of the channel, up to 0.2 kcal/mol (Fig. 6 *d*). It should also be noted that the o1 configuration stabilizes more than the i1 destabilizes because it is closer to the center of the channel (Fig. 1).

DISCUSSION

We find a variety of energetically accessible Trp conformations for gramicidin A. In particular, conformations 2 and 8 are both within 1.3 kcal/mol of conformation 1. The outward pointing conformations yield a negative potential within the channel. For the o1 and o2 conformations, the potential reaches a minimum in the center at about −0.5 kcal/mol per opposing pair of Trps (Fig. 6), whereas for the i and p conformations the potential is positive and peaks in the center. The images contribute about −0.2 kcal/mol for the four pairs, all in o1 configurations (conformation 1, Fig. 4 *a*). We first compare our conformational search results to those of Venkatachalam and Urry (1983) and to the structural constraints provided by 2D NMR, Raman spectroscopy, and solid-state NMR. Then we describe briefly how the Trp PMF could affect channel conductance. Finally, the magnitude and shape of the interaction potential are compared to similar estimates based on experimental data (Hu and Cross, 1995) for a continuum dielectric model (Sancho and Martínez, 1991), for a left-handed gramicidin A atomistic model with polarization (Etchebest and Pullman, 1985), and for a right-handed gramicidin A atomistic model without polarization but with dynamic averages (Woolf and Roux, 1997).

Implications of conformational search results

Our Trp side-chain conformational search for the right-handed helix is similar to that of Venkatachalam and Urry (1983) (the VU search) for left- and right-handed helices. However, it is difficult to compare our results to the VU results directly, because the set of acceptable conformations described there pertains to the left-handed helix, with only the lowest-energy conformation being described for the right-handed helix. Tryptophans with identical rotameric states point in opposite directions in left- and right-handed helices (Nicholson and Cross, 1989), making it impossible to ascertain from the set of accessible conformations in left-handed helices what rotameric states would be accessible or inaccessible in right-handed helices. The lowest energy state for right-handed helices in VU contains, using the classification relationships shown in Table 3, i1, o2, o2, and o2 for Trp^9, Trp^{11}, Trp^{13}, and Trp^{15}, respectively. The o2 conformation is sufficiently less favorable energetically than the o1 conformation that this VU conformation does not appear among the top seven of our group 1 conformations. However, i1 and o2 at position 9 are found to be nearly as favorable as o1, provided the other three Trps are in the o1 conformation (compare conformations 2 and 8 to conformation 1 in Table 1).

In both this and the VU studies, only the conformational energy was accounted for, leaving unanswered the question of how interactions with the lipid-water environment affect conformation. It is noteworthy that conformation 1 corresponds to an acceptable solid-state NMR structure (Table 4; Hu et al., 1993, 1995; Koeppe et al., 1994; Ketchem et al., 1997), and conformation 2, of similar energy, corresponds to the SDS micelle conformation (Table 4; Arseniev et al., 1986a, 1990; Lomize et al., 1992). This suggests that the

TABLE 3 Trp side-chain conformation classification schemes for right-handed β-helices

Canonical* χ^1	−60	180	180	−60	+60	+60
Canonical $\chi^{2,1}$	−90	+90	−90	+90	−90	+90
Venkatachalam and Urry (1983)	d	c,j	a,b	e	f,g	i,k
Takeuchi et al. (1990)	G′−	T+	T−	G′+	G−	G+
Hu et al. (1995)	IA, IIA	IB, IIB				
Current work	o1	o2	i1	i2	p1	p2

*Actual values of defined conformations differ from the canonical values. For example, $\chi^{2,1}$ is 60, 120 or −60, −120 in the Venkatachalam and Urry search, canonical (±90) in the Takeuchi et al. (1990) classification scheme, but ±96 in the Muruyama and Takeuchi (1997) refinement, and ±97 (Group I) or ±46 (Group II) in the Hu et al. (1995) classification. Others have deduced dihedral angles, but have not suggested classifications (Koeppe et al., 1994; Arseniev et al., 1986b; Lomize et al., 1992).

TABLE 4 Measured possible values for gramicidin A channel Trp dihedrals*

	Trp^9		Trp^{11}		Trp^{13}		Trp^{15}	
	χ^1	$\chi^{2,1}$	χ^1	$\chi^{2,1}$	χ^1	$\chi^{2,1}$	χ^1	$\chi^{2,1}$
Arseniev et al. (1990)	167	89	−65	−53	−67	−91	−69	−93
Koeppe et al. (1994)#	−100	−91	−65	−96				
	−166	92	170	95				
Hu et al. (1995)#	−72	−97	−70	−81	−63	−90	−58	−96
	174	97	171	81	169	90	165	96
Maruyama and Takeuchi (1997)		±97		±95		±95		±95
Ketchem et al. (1997)	−74	−82	−71	−91	−64	−85	−61	−90

*Preliminary estimates are not included when refined values were published subsequently, except in the case of Hu et al. (1995), which is included to emphasize that both o1 and o2 conformations are allowed by solid-state NMR, as was also found by Koeppe et al. (1994).
#Only two of the four sets of dihedrals allowed by solid-state NMR are included here; the other two are disallowed by the Raman results.

observed Trp conformations in gA are governed primarily by interactions within the peptide. For conformation 8, the interactions with the environment should differ from those of conformations 1 and 2 because the dipole and hydrophobic pole of the indole in Trp^9 are rotated by ~180°, and it therefore may be a less favorable conformation than the conformational energy alone suggests.

Other than conformations 1, 2, and 8, no alternative conformations should be observed unless interactions with the interface stabilize an otherwise unlikely conformation by 5 kcal/mol or more. This seems unlikely to happen because the o conformations should be more stabilized by the interface than i or p because of hydrogen bonding of indole N-Hs with bulk water, alignment of the indole dipole with the interfacial dipole potential (in uncharged bilayers), and hydrophobicity of the benzene ring. The conformational energy of o2 is much less favorable than that of o1 (compare conformations 3 and 4 to conformation 1, for example), except in Trp^9. Therefore, it is unlikely that any conformation would be preferred over o1, except in Trp^9.

The o1 conformations from all of our structures (Table 2) conform quite well with those determined by NMR and Raman spectroscopy (Table 4), except for discrepancies of 20–30°in the $\chi^{2,1}$ angles, which have measured magnitudes of ~90°. These discrepancies may be due to neglect of interactions with the interface or differing assumptions about the backbone structure. It should also be noted here that based on steric conflicts, Hu and Cross (1995) rule out two of the possible four combinations of o1 and o2 for the Trp^9/Trp^{15} pair, o1/o2 and o2/o2. We do not rule these out based on steric conflicts. The o1/o2 combination appears in conformations 3, 7, 24, 26, 28, and 30 and o2/o2 in conformation 6. However, these conformations probably do not conform to the constraints imposed by the NMR data. The torsion angles from our search vary from allowed torsion angles deduced by Hu et al. (1995), as shown in Table 5.

The exclusion of o2 for Trp^{11} (Table 2) in our search deserves some comment. We suppose that there must have been a conflict with neighboring Leu's in the initial structure that was not resolved by the initial minimization of the non-Trp side chains. We say this because in the Venkatachalam and Urry (1983) study, o2 was the preferred conformation for Trp^{11} in the right-handed helix. This implies that our method was not quite exhaustive and may have been improved by a Monte Carlo or simulated annealing approach (e.g., Lee et al., 1998) that could more readily allow the system to surmount such local barriers. Likewise, other excluded conformations (i1 for Trp^{15}; i2 for Trp^{11}; p1 for Trp^9, Trp^{13}, and Trp^{15}; and p2 for all residues) may be accessible, although it appears likely that they would be energetically less favorable, given the appearance order of i1, i2, and p1 in Table 1.

The population distribution of minor rotameric states for gramicidin A tryptophans is not yet known. Fluorescence polarization in DMPC bilayers is high compared to that in dioleoylphosphatidylcholine (DOPC) bilayers, but decreases dramatically with increased pressure (Scarlata, 1991). This is interpreted to imply that the side-chain conformational mobility is much higher in DOPC than in thinner DMPC bilayers and becomes larger in DMPC at higher pressures, because of increased bilayer thickness, presumably because of loss of stabilizing contacts between Trp side chains and lipid headgroups (or water) for thicker bilayers. In addition, fluorescence anisotropy decreases steeply with temperature above the DMPC gel-liquid transition temperature (Scarlata, 1988), which was interpreted to suggest a

TABLE 5 Trp^9 and Trp^{15} dihedrals rejected by Hu and Cross (1995) on steric grounds compared to the mean of the two monomer angles for those of the same conformers accepted by the current search

		Trp^9		Trp^{15}	
		χ^1	$\chi^{2,1}$	χ^1	$\chi^{2,1}$
Hu and Cross rejects*	o1/o2	−72	−97	165	96
	o2/o2	174	97	165	96
Conform. 3	o1/o2	−67	−70	−179	84
Conform. 7	o1/o2	−69	−62	−178	85
Conform. 24	o1/o2	−68	−62	−179	85
Conform. 26	o1/o2	−68	−73	−178	86
Conform. 28	o1/o2	−69	−62	−178	85
Conform. 30	o1/o2	−70	−63	−179	86
Conform. 6	o2/o2	−174	92	−173	91

*Conformations that fit the solid-state NMR result, but are rejected on steric grounds.

temperature-induced access to alternative conformational states as Trp-lipid contacts are removed by increased temperature. Gramicidin A fluorescence lifetime measurements yielded a minimum of four exponential phases (Suzanne F. Scarlata, personal communication), indicating either that multiple Trp conformations exist on the nanosecond time scale or that at least four of the Trps in the gramicidin A channel are in very different environments.

The dominant structure has been limited to two possible configurations for Trp side chains because of the narrowness of the Raman spectrum indole bands, with the value of the Trp $\chi^{2,1}$ angle within 6° of ±94° (Takeuchi et al., 1990; Maruyama and Takeuchi, 1997). Solid-state NMR analysis of the N-H angle with respect to the magnetic field in DMPC multilayers, excluding sterically impossible structures and those not consistent with the Raman result, also limit the conformations for the dominant state to two conformations corresponding approximately to o1 and o2, both in studies of only Trp^9 and Trp^{11} (Koeppe et al., 1994) and in studies of all four Trps (Hu et al., 1993, 1995; Hu and Cross, 1995).

Given the conformational energies in Table 2, it appears that o1 should be highly preferred for Trp^{11}, Trp^{13}, and Trp^{15}, but that both o1 and o2 should be populated for Trp^9. There is evidence in quadrupole splitting and cryogenic NMR studies that the side chains are not significantly distributed between o1 and o2 conformations (Tim Cross, personal communication). Moreover, the 2D NMR results should show distinct N-Cα-Cβ-H vicinal couplings for o1 and o2, because in o2 both Cβ hydrogens are close to the peptide N, whereas in o1 only one is close, yet no data showing the coexistence of these distinct conformations have been observed. Only the couplings for o1 are observed for Trp^{11}, Trp^{13}, and Trp^{15}; only the couplings for o2 are observed for Trp^9 (Arseniev et al., 1985). Acylation of the ethanolamine terminus causes a loss of shielding of Leu^{10} by Trp^9 in SDS micelles and a change in Trp^9 deuterium splitting in DMPC multilayers, indicating a change in Trp^9 configuration from the o2 to the o1 conformation (Koeppe et al., 1995, 1996). Nevertheless, our conformational energy results imply that the question is still open. Solid-state NMR evidence argues against any change in Trp conformation upon cation binding (Separovic et al., 1994), whereas the Trp indole N deuteration rate increases by a factor of nearly 1.75 for Trp^{11} and decreases by a factor of 0.71 for Trp^{13} upon cation binding (Maruyama and Takeuchi, 1997).

Although studies of protein and peptide Trp libration frequency and amplitude using fluorescence spectroscopy have illuminated motions within a single side-chain conformation on the nanosecond time scale (Axelsen et al., 1988; Demchenko, 1988; Ovstrovsky et al., 1988; Weaver et al., 1988; Scarlata, 1988; Axelsen and Prendergast, 1989; Scarlata, 1991), the time scale for interconversion between Trp conformations in gramicidin A is unknown. The solid-state NMR time scale allows identification of gramicidin A Val side-chain conformation interconversions on the nanosecond to microsecond time scale in the cases of Val^1 and Val^7, fixed on the microsecond time scale for Val^6 and Val^8 (Lee et al., 1995), but none are observed for Trp side chains. If frequent (e.g., on the microsecond time scale) interconversion occurred between o1 and o2 states, powder pattern profiles would reflect much greater averaging (Hu et al., 1995). Conformational changes on millisecond or slower time scales are not detectable by this approach, but if they were to occur, multiple sets of resonances would be observed in the spectra of oriented samples (Tim Cross, personal communication).

Implications of Trp-ion PMF for ion conductance

The energies of all but the three most stable conformations, 1, 2, and 8, are too high to allow observation unless 1) the Trp rotamers are stabilized by interactions with the environment (not included in our computation), or 2) the Trp rotamers are confined to metastable states by high barriers to interconversion. Although the likelihood of either possibility is uncertain, if multiple stable conformations were to occur, one would expect from our PMF calculations that several conductance levels would result. With all four Trps in the o conformation, the Trps and their images stabilize an ion in the center of the channel, the expected location of the rate-limiting barrier to ion passage, by ~2 kcal/mol (Fig. 4 *a*). This stabilization is reduced to 0.8 kcal/mol (with bulk water polarization; Fig 4 *d*, *no symbols*) if two pairs of Trps are in the i configuration (conformation 46), so that the underlying central barrier, ΔG_{trans}, would be increased by $\sim 2kT$ (uncorrected; see below). In the absence of other rate-limiting steps, the conductance of such a channel would be 7.4-fold lower on the assumption that the conductance is proportional to $\exp(-\Delta G_{trans}/kT)$. We conclude that if such conformational changes occur with lifetimes greater than milliseconds and in small enough populations so as to be undetectable by NMR, they should be readily detectable with single-channel current measurements.

These PMF calculations are also in qualitative agreement with measurements of single-channel conductances for Trp-Phe replacement analogs by Becker et al. (1991), who found that gA analog channel conductances were decreased in increments as the total number of Trps was reduced from 8 to 6, 4, or 2, rather independently of which combination of Trps was replaced. Likewise, our results can be used to interpret recent experiments with indole-5 fluorinated Trp side chains (Andersen et al., 1998; Busath et al., 1998), in which an increase in the Trp side chain dipole moment enhances conductance under conditions where translocation is rate limiting.

Comparison to previous estimates of the Trp PMF

Hu and Cross (1995) analyzed the Becker et al. (1991) data, assuming a solid-state NMR Trp conformation (type o1), indole dipoles (Weiler-Feilschenfeld et al., 1970), and the

relationship between $\exp(-\Delta G_{trans}/kT)$ and conductance mentioned above. Based on that relationship, they conclude that the effective dielectric constant shielding the ion-Trp interaction is 5.1 and that the interaction energy for pairs of Trp^9, Trp^{11}, and Trp^{13} is -0.28, -0.40, and -0.37 kcal/mol, respectively (derived from the first three lines of their table 3).

Sancho and Martínez (1991) compute the Trp PMF representing the group of Trps as a radially symmetrical dipolar annulus embedded in a two-component dielectric continuum where the bath and pore waters are assigned $\epsilon = 80$ and the channel wall and lipid are assigned $\epsilon = 2$. With the annulus positioned near the ends of the channel, the PMF shapes for outward and radial dipole positions, the latter being parallel to the plane of the bilayer (like p1) but projecting away from the channel rather than tangential to it, are similar to those reported here for the o1 and p1 conformations, respectively. The energies of interaction between an outward pointing (perfectly axial) annular dipole of 1 D positioned 7.0 or 11.5 Å from the channel center (the approximate positions of Trp^9 and Trp^{15}) and a cation at the center of the channel are -0.22 or -0.26 kcal/mol, respectively (converted from millivolts, as read from their figure 6a).

Etchebest and Pullman (1985) compute the potential energy profile for a cation moving through a gA channel with and without the side chains, using an empirical force field that lacks bond and angle stretching terms, but includes polarization energy. Although not stated, it appears that the charges on the Trp side chains corresponded to the Weiler-Feilschenfeld et al. (1970) indole dipoles and that the channel is in a vacuum, i.e., with $\epsilon = 1$. They used a variant of the left-handed global minimum VU conformation, in which Trp^9 and Trp^{15} are in an i1-like conformation and Trp^{11} and Trp^{13} are in an o2-like conformation. Unlike our PMFs and those of Sancho and Martínez (1991), the electrostatic component of the ion-side chain interaction energy varied widely from -2.9 to $+2.2$ kcal/mol, but the polarization energy was uniformly negative and ranged smoothly from -3.7 to -4.7 kcal/mol in the channel, and was -3.7 kcal/mol in the center of the channel. The total polarization energy is negative throughout the channel, adding a constant component to the PMF, because the cation polarizes the indole π clouds in a way that favors their interaction independent of their orientation.

Finally, Woolf and Roux (1997) averaged the axial electrostatic PMF from each of the gA side chains for each frame of a CHARMM molecular dynamics simulation of the channel in a dimyristoyl phosphatidylcholine bilayer. The parameters for the channel, including the side-chain partial charges, were presumably identical with those used here, although it is not stated what nonbonded cutoffs were used. In the dynamic trajectory, the side chains fluctuated about unique average positions consistent with solid-state NMR Trp chemical shifts, dipole coupling, and quadrupole splitting data, presumably o1. Their traces should then be directly comparable to our traces for the o1 conformation (*without symbols*) in Fig. 6, except that they used a dielectric constant of 1 (Benoit and Roux, personal communication), resulting in twofold greater energies, and they did not use images, which have a smaller effect. In general, the shapes of the average dynamic PMF are similar to those reported here, with the Trp^{13} and Trp^{15} producing a broader well. However, unlike our result, the four Trps vary considerably in the maximum depth of the PMF, reaching approximately -1.8, -1.5, -1.0, and -1.0 kcal/mol for Trp^9, Trp^{11}, Trp^{13}, and Trp^{15}, respectively, whereas ours (with images and $\epsilon = 2$) are all -0.5 kcal/mol. Furthermore, there are larger humps in the center of the profiles for the dynamic PMFs. The central humps and deeper PMF wells near the binding site for Trp^9 and Trp^{11} are indicative of more radially oriented dipoles in the dynamic structure.

The Trp PMF at the center of the channel of -1.8 kcal/mol for all eight Trps (Fig. 4 *a*) or -0.5 kcal/mol per pair (Fig. 6) must be corrected because of the low dipole moment of the toph19 Trp indole to allow a meaningful comparison to the values from the other three approaches. Neglecting the 7° error in the orientation of the dipole, the interaction energies should be scaled up by a factor of 1.80 to be consistent with the Weiler-Feilschenfeld et al. (1970) indole dipole moment of 2.08. This yields -0.9 kcal/mol per pair of Trps. Our value is more negative than the -0.28 to -0.40 determined by Hu and Cross (1995), probably because we used a 2.5-fold lower effective dielectric constant than they deduced. Our dielectric constant is probably too low, but theirs would be overestimated if the assumption that translocation is strictly the rate-limiting process is incorrect. For instance, if the entry process begins to limit the flux, the dipole effects on the central barrier become less effectual (Busath et al., 1998), which is misinterpreted as higher dielectric shielding of the Trp dipole. Our value is more negative than the Sancho and Martínez prediction of -0.44 to -0.52 kcal/mol (after scaling their axial dipole up by a factor of 2 to be consistent with the Weiler-Feilschenfeld et al. (1970) indole dipole, taken together with the Hu and Cross (1995) estimates of the axial component of the indole dipole in the solid-state NMR structure). This is probably due to the additional shielding by pore water in their computation, in which the pore volume is assigned a dielectric constant of 80, which now appears to be too high because of water polarization in the pore (Partenskii et al., 1991). The shape of the electrostatic potential in the Etchebest and Pullman (1985) PMF is quite irregular compared to ours. In part this may be due to the combination, in their Trp conformation, of two pairs of inward and two pairs of outward pointing side-chain dipoles. But our conformation 31 and 46 PMFs (Fig. 4, *c* and *d*), with similar mixtures of side chain conformations, are not as irregular. Therefore, no quantitative comparison can be made, except to say that the extrema in their PMF have somewhat larger magnitudes than ours, probably because $\epsilon = 1$ in their calculations compared to 2 in ours. However, they demonstrated that the Trp polarization contributes a flat PMF inside the channel, with little impact on the shape of the PMF inside the

channel, despite their mixture of Trp side chain conformations, and polarization can therefore be neglected to a first approximation. We estimate, then, that the ion-Trp interaction energy is probably about −0.9 kcal/mol per pair, assuming that the backbone and pore waters present an effective dielectric constant of ~2.

CONCLUSIONS

Our calculations and the available experimental data are best explained by a gramicidin conformer having all four pairs of Trp side-chain dipoles pointing outward. Each pair stabilizes the ion in the center of the channel by a similar amount. Alternative dipole orientations for Trp^9 also appear to be likely. The Trp dipole is sufficient to explain effects of Trp mutations on ion transport. The analysis of how noncontact dipoles affect channel permeation is expected to be helpful in gaining an understanding of other narrow channels such as the voltage-gated potassium channel.

We thank Suzanne F. Scarlata, James F. Hinton, and Timothy A. Cross for helpful discussions.

This project was partially funded by National Institutes of Health grant R01 AI23007.

REFERENCES

Andersen, O. S., D. Greathouse, L. L. Providence, M. D. Becker, and R. E. Koeppe II. 1998. Importance of tryptophan dipoles for protein function. 5-Fluorination of tryptophans in gramicidin A channels. *J. Am. Chem. Soc.* 120:5142–5146.

Andersen, O. S., and R. E. Koeppe II. 1992. Molecular determinants of channel function. *Physiol. Rev.* 72:S89–S158.

Arseniev, A. S., I. L. Barsukov, V. F. Bystrov. 1986a. Conformation of gramicidin A in solution and micelles: two dimensional 1-H NMR study. *In* Chemistry of Peptides and Proteins, Vol. 3. W. Voelter, E. Bayer, Y. A. Ovchinnikov, and V. T. Ivanov, editors. Walter de Gruyter and Co., New York. 127–158.

Arseniev, A. S., I. L. Barsukov, V. F. Bystrov, A. L. Lomize, and Y. A. Ovchinnikov. 1985. H-NMR study of gramicidin A transmembrane ion channel. *FEBS Lett.* 186:168–174.

Arseniev, A. S., A. L. Lomize, I. L. Barsukov, and V. F. Bystrov. 1986b. Gramicidin A transmembrane ion-channel. Three-dimensional structure reconstruction based on NMR spectroscopy and energy refinement. *Biol. Membr.* 3:1077–1104.

Arseniev, A. S., A. L. Lomize, I. L. Barsukov, and V. F. Bystrov. 1990. Gramicidin A transmembrane channel. Three-dimensional structural rearrangement based on NMR spectroscopy and energy refinement. *Biol. Membr.* 3:1723–1778.

Axelsen, P. H., C. Haydock, and F. G. Prendergast. 1988. Molecular dynamics of tryptophan in ribonuclease-T1. I. Simulation strategies and fluorescence anisotropy decay. *Biophys. J.* 54:249–258.

Axelsen, P. H., and F. G. Prendergast. 1989. Molecular dynamics of tryptophan in ribonuclease-T1. II. Correlations with fluorescence. *Biophys. J.* 56:43–66.

Bamberg, E., K. Noda, E. Gross, P. Läuger. 1976. Single-channel parameters of gramicidin A, B, and C. *Biochim. Biophys. Acta.* 419:223–228.

Becker, M. D., D. V. Greathouse, R. E. Koeppe II, and O. S. Andersen. 1991. Amino acid sequence modulation of gramicidin channel function: effects of tryptophan-to-phenylalanine substitutions on the single-channel conductance and duration. *Biochemistry.* 30:8830–8839.

Brooks, B. R., R. E. Bruccoleri, B. D. Olafson, D. J. States, S. Swaminathan, and M. Karplus. 1983. CHARMM: a program for macromolecular energy, minimization, and dynamics calculations. *J. Comput. Chem.* 4:187–217.

Busath, D. D. 1993. The use of physical methods in determining gramicidin channel structure and function. *Annu. Rev. Physiol.* 55:473–501.

Busath, D. D., C. D. Thulin, R. W. Hendershot, L. R. Phillips, P. Maughn, C. D. Cole, N. C. Bingham, S. Morrison, L. C. Baird, R. J. Hendershot, M. Cotten, and T. A. Cross. 1998. Non-contact dipole effects on channel permeation. I. Experiments with (5F-indole)Trp-13 gramicidin A channels. *Biophys. J.* 75:2830–2844.

Demchenko, A. P. 1988. Red-edge-excitation fluorescence spectroscopy of single-tryptophan proteins. *Eur. Biophys. J.* 16:121–129.

Dilger, J. P. 1981. The thickness of monoolein lipid bilayers as determined from reflectance measurements. *Biochim. Biophys. Acta.* 645:357–363.

Etchebest, C., and A. Pullman. 1985. The effect of amino-acid side chains on the energy profiles for ion transport in the gramicidin A channel. *J. Biomol. Struct. Dyn.* 2:859–870.

Hao, Y., M. R. Pear, and D. D. Busath. 1997. Molecular dynamics study of free energy profiles for organic cations in gramicidin A channels. *Biophys. J.* 73:1699–1716.

Heitz, F., P. Daumas, N. Van Mau, R. Lazaro, Y. Trudelle, C. Etchebest, and A. Pullman. 1988. Linear gramicidins: influence of the nature of the aromatic side chains on the channel conductance. *In* A. Pullman, J. Jortner, and B. Pullman, editors. Transport Through Membranes: Carriers, Channels, and Pumps. Kluwer Academic Publishers, Boston. 147–165.

Heitz, F., C. Gavach, G. Spach, and Y. Trudelle. 1986. Analysis of the ion transfer through the channel of 9,11,13,15-phenylalanylgramicidin A. *Biophys. Chem.* 24:143–148.

Heitz, F., G. Spach, and Y. Trudelle. 1982. Single channels of 9, 11, 13, and 15-destryptophyl-phenylalanyl-gramicidin A. *Biophys. J.* 40:87–89.

Hu, W., and T. A. Cross. 1995. Tryptophan hydrogen bonding and electrical dipole moments: functional roles in the gramicidin channel and implications for membrane proteins. *Biochemistry.* 34:14147–14155.

Hu, W., N. D. Lazo, and T. A. Cross. 1995. Tryptophan dynamics and structural refinement in a lipid bilayer environment: solid state NMR of the gramicidin channel. *Biochemistry.* 34:14138–14146.

Hu, W., K. C. Lee, and T. A. Cross. 1993. Tryptophans in membrane proteins: indole ring orientations in the gramicidin channel. *Biochemistry.* 32:7035–7047.

IUPAC-IUB Commission. 1970. Abbreviations and symbols for the description of the conformation of polypeptide chains. *J. Mol. Biol.* 52: 1–17.

Iverson, G., Y. I. Kharkats, and J. Ulstrup. 1998. Simple dielectric image charge models for electrostatic interactions in metalloproteins. *Mol. Phys.* 94:297–306.

Jones, D., E. Hayon, and D. Busath. 1986. Tryptophan photolysis is responsible for gramicidin-channel inactivation by ultraviolet light. *Biochim. Biophys. Acta.* 861:62–66.

Jordan, P. C. 1984. The total electrostatic potential in a gramicidin channel. *J. Membr. Biol.* 78:91–102.

Jordan, P. C., R. J. Bacquet, J. A. McCammon, and P. Tran. 1989. How electrolyte shielding influences the electrical potential in transmembrane ion channels. *Biophys. J.* 55:1041–1052.

Ketchem, R. R., K. C. Lee, S. Huo, and T. A. Cross. 1996. Macromolecular structural elucidation with solid-state NMR-derived orientational constraints. *J. Biomol. NMR.* 8:1–14.

Ketchem, R. R., B. Roux, and T. A. Cross. 1997. High-resolution polypeptide structure in a lamellar phase lipid environment from solid state NMR derived orientational constraints. *Structure.* 5:1655–1669.

Killian, J. A. 1992. Gramicidin and gramicidin/lipid interactions. *Biochim. Biophys. Acta* 1113:391–425.

Koeppe, R. E., II, J. A. Killian, and D. V. Greathouse. 1994. Orientations of the tryptophan 9 and 11 side chains of the gramicidin channel based on deuterium nuclear magnetic resonance spectroscopy. *Biophys. J.* 66:14–24.

Koeppe, R. E., II, J. A. Killian, T. C. B. Vogt, B. de Kruijff, M. J. Taylor, G. L. Mattice, and D. V. Greathouse. 1995. Palmitoylation-induced conformational changes of specific side chains in the gramicidin transmembrane channel. *Biochemistry.* 34:9299–9306.

Koeppe, R. E., II, T. C. B. Vogt, D. V. Greathouse, J. A. Killian, and B. de Kruijff. 1996. Conformation of the acylation site of palymitolygramicidin in lipid bilayers of dimyristoylphosphatidylcholine. *Biochemistry.* 35:3641–3648.

Lee, J., H. A. Scheraga, and S. Rackovsky. 1998. Conformational analysis of the 20-residue membrane-bound portion of melittin by conformational space annealing. *Biopolymers.* 46:103–115.

Lee, K. C., S. Huo, and T. A. Cross. 1995. Lipid-peptide interface: valine conformation and dynamics in the gramicidin channel. *Biochemistry.* 34:857–867.

Lomize, A. L., V. Y. Orekhov, and A. S. Arseniev. 1992. Refinement of the spatial structure of the ionic channel of gramicidin A. *Bioorg. Khimiya.* 18:182–200 (in Russian).

Maruyama, T., and H. Takeuchi. 1997. Water accessibility to the tryptophan indole N-H sites of gramicidin A transmembrane channel: detection of positional shifts of tryptophans 11 and 13 along the channel axis upon cation binding. *Biochemistry.* 36:10993–11001.

Neumcke, B., and P. Läuger. 1969. Nonlinear electrical effects in lipid bilayer membranes. *Biophys. J.* 9:1160–1170.

Nicholson, L. K., and T. A. Cross. 1989. Gramicidin cation channel: an experimental determination of the right-handed helix sense and verification of the β-type hydrogen bonding. *Biochemistry.* 28:9379–9385.

Ovstrovsky, A. V., L. P. Kalinichenko, V. I. Emelyanenko, A. V. Klimanov, and E. A. Permyakov. 1988. Environment of tryptophan residues in various conformational states of α-lactalbumin studied by time-resolved and steady-state fluorescence spectroscopy. *Biophys. Chem.* 30:105–112.

Partenskii, M. B., M. Cai, and P. C. Jordan. 1991. A dipolar chain model for the electrostatics of transmembrane ion channels. *Chem. Phys.* 153: 125–131.

Pickar, A. D., and R. Benz. 1978. Transport of oppositely charged lipophilic probe ions in lipid bilayer membranes having various structures. *J. Membr. Biol.* 44:353–376.

Richardson, J. S., and D. C. Richardson. 1989. Principles and patterns of protein conformation. *In* Prediction of Protein Structure and the Principles of Protein Conformation. Gerald D. Fasman, editor. Plenum Press, New York. 1–98.

Roux, B., and M. Karplus. 1988. The normal modes of the gramicidin-A dimer channel. *Biophys. J.* 53:297–309.

Sancho, M., and G. Martínez. 1991. Electrostatic modeling of dipole-ion interactions in gramicidin like channels. *Biophys. J.* 60:81–88.

Scarlata, S. 1988. The effects of viscosity on gramicidin tryptophan rotational motion. *Biophys. J.* 54:1149–1157.

Scarlata, S. 1991. Effect of increased chain packing on gramicidin-lipid interactions. *Biochemistry.* 30:9853–9859.

Separovic, F., J. Geehrmann, T. Milne, B. A. Cornell, S. Y. Lin, and R. Smith. 1994. Sodium ion binding in the gramicidin A channel: solid-state NMR studies of the tryptophan residues. *Biophys. J.* 67:1495–1500.

Sham, Y. Y., I. Muegge, and A. Warshel. 1998. The effect of protein relaxation on charge-charge interactions and the dielectric constant of proteins. *Biophys. J.* 74:1744–1753.

Simonson, T. 1998. Dielectric constant of cytochrome *c* from simulations in a water droplet including all electrostatic interactions. *J. Am. Chem. Soc.* 120:4875–4876.

Smythe, W. R. 1967. Static and Dynamic Electricity, 3rd Ed. McGraw-Hill, New York. 179–208.

Takeuchi, H., Y. Nemoto, and I. Harada. 1990. Environments and conformations of tryptophan side chains of gramicidin A in phospholipid bilayers studied by Raman spectroscopy. *Biochemistry.* 29:1572–1579.

Turano, B., M. Pear, and D. Busath. 1992. Gramicidin channel selectivity. Molecular mechanics calculations for formamidinium, guanidinium, and acetamidinium. *Biophys. J.* 63:152–161.

Venkatachalam, C. M., and D. W. Urry. 1983. Theoretical conformational analysis of the gramicidin A transmembrane channel. I. Helix sense and energetics of head-to-head dimerization. *J. Comp. Chem.* 4:461–469.

Waldbillig, R. C., and G. Szabo. 1979. Planar bilayer membranes from pure lipids. *Biochim. Biophys. Acta.* 557:295–305.

Weaver, A. J., M. D. Kemple, and F. G. Prendergast. 1988. Tryptophan sidechain dynamics in hydrophobic oligopeptides determined by use of ^{13}C nuclear magnetic resonance spectroscopy. *Biophys. J.* 54:1–15.

Weber, E. 1965. Electromagnetic Theory: Static Fields and their Mapping. Dover, New York.

Weiler-Feilschenfeld, H., A. Pullman, H. Berthod, and C. Giessner-Prettre. 1970. Experimental and quantum mechanical studies of the dipole moments of quinoline and indole. *J. Mol. Struct.* 6:297–304.

Woolf, T. B., and B. Roux. 1997. The binding site of sodium in the gramicidin A channel: comparison of molecular dynamics with solid-state NMR data. *Biophys. J.* 72:1930–1945.

Woolley, G. A., and B. A. Wallace. 1992. Model ion channels—gramicidin and alamethicin. *J. Memb. Biol.* 129:109–136.